Mechanics of Roller Chain Sprocket Contact

Mahn Shik Kim

Glen E. Johnson

Design Laboratory, Mechanical Engineering, and Applied Mechanics

University of Michigan, Ann Arbor, MI 48109-2125

ens7

UMR1128

Mechanics of Roller Chain-Sprocket Contact[1]

Mahn Shik Kim[2]

Glen E. Johnson

Design Laboratory, Mechanical Engineering and Applied Mechanics,

University of Michigan, Ann Arbor, MI 48109-2125

Abstract

The contact phenomenon between a roller chain and sprocket was investigated using a new mathematical model which, unlike previous models, made it possible to predict the load distribution without resorting to assumptions about the distribution of the contact points. It was found that the distribution of contact points on the sprocket is affected by the external loading condition, and this relationship was determined. Effects of friction and the dimensional variations in the chain pitch and the sprocket pitch were also investigated. Link tension predicted by the simulation showed excellent agreement with experimental data reported by Naji and Marshek.

---

[1]This article is based on the Ph. D. dissertation submitted by the first author to the Rackham Graduate School at the University of Michigan, 10/90.

[2]Currently employed as a researcher at the Technical Center, Daewoo Motor Company, Inchon, Korea.

1 INTRODUCTION

An extensive analysis of the contact phenomenon occurring between the roller chain and the sprocket can be found in Binder's classical textbook [1] published in 1956. In the early 1980's, Naji and Marshek [2, 3, 4] complemented Binder's work by theoretical and experimental investigation of the contact phenomenon under quasi-static conditions. The kinematics of the roller chain drive are quite complicated due to non-trivial geometry of the sprocket tooth, manufacturing tolerance, and the possible change in clearances between components caused by wear. Several simplifying assumptions on the geometry of the roller chain drive were made in previous studies.

The geometry of the sprocket tooth standardized by ANSI [5] is defined by four different curvatures as shown in Fig. 1.1. The curve which is at the bottom of the tooth form is often called the seating curve while the curves next to the seating curve are called working curves. The radius of the seating curve is designed, in the ANSI standard, to be slightly bigger than that of the roller. Therefore, the trajectory of the center of the roller on the seating curve is still a circular arc, although the radius of the arc is very small relative to that of the roller.

The curvature difference between the roller and the seating curve was neglected in previous models and, therefore, the trajectory of the center of the roller on the seating curve shrank to a point instead of a circular arc as shown in Fig. 1.2 (a). Consequently, the angle of the resultant normal contact force applied on the roller by the sprocket could not been determined from physical reasoning by most models. One exception to this is the "stiff link - soft tooth" model devised by Gerbert [8].

Binder assumed that the angle of the contact force on each tooth with respect to the tooth is constant. But he made no comment on how to determine the value. In the model

of Naji and Marshek a number of rollers on the high tension side contact the tight side tooth flanks and the rest contact the slack tooth flanks. It was further assumed in their model that, if the roller contacts the seating curve, the angle of the normal contact force is constant with respect to axis of the symmetry of the tooth form. The value of the pressure angle used in the theoretical prediction of Naji and Marshek on the chain tension was selected to provide good agreement with their experimental data.

The angles of normal contact forces on the sprocket strongly affect the distribution of contact forces and chain link tensions. It will be shown that in a reliable roller chain drive the rollers contact not only the working curve but also the seating curve. Therefore, the angle of the normal contact force not only on the working curve but also on the seating curve should be precisely estimated to correctly predict the load distribution of the chain and the sprocket.

A new model which enables us to determine the load distribution without resorting to any assumption on the distribution of the contact points is developed. It is shown that the distribution of the contact points on the sprocket is in fact determined by the loading condition. In the new model the curvature difference is included and the trajectory of the center of the roller on the seating curve composes a circular arc as shown in Fig. 1.2 (b). Refined modeling of the friction forces is also incorporated.

2 DISTRIBUTION OF CONTACT POINTS

In this section, the geometric relationship between contact points on the sprocket surfaces is derived. Only steel roller chains and steel sprockets standardized by ANSI are considered. The chain and the sprocket are regarded as two-dimensional bodies and any variation in the direction parallel to the axis of the rotation of the sprocket is neglected. Furthermore, point contact is assumed and the effects of elastic deformation of the chain and the sprocket are neglected.

The tolerances on the chain pitch and the sprocket pitch are not given by the standard explicitly. However, they can be computed from the tolerances on the chain length and the sprocket diameter given by the standard. New chain should have an over-length error, and the error in the length increases in the course of operation because of wear between the pin and the bushing. On the other hand, the error in the sprocket pitch can be either negative or positive. The effect of a negative error in the sprocket pitch is similar in many aspects to that of a positive error of the same magnitude in the chain pitch. The tolerance on the sprocket pitch turns out to be, in general, larger than the tolerance on the chain pitch. (Detailed treatment of the tolerances on the chain pitch and the sprocket pitch can be found in Kim [7].) Therefore, the error in the sprocket pitch should be also considered whenever the effects of the error in the chain pitch are discussed.

The system to be handled here consists of a sprocket and a segment of endless chain wrapping the sprocket as shown in Fig. 2.1. Without loss of generality it can be assumed that the sprocket rotates counter-clockwise. Each roller and each link is given an integer index for convenient mathematical manipulation. Roller 1 is defined as the roller that has most recently come in contact with the sprocket. Roller 1 is located at the end of the high tension side for the driver sprocket, whereas it is at the end of the low tension side for the driven sprocket. The roller j follows roller $j+1$ in the direction of rotation of the sprocket. m is the instantaneous number of rollers in contact with the sprocket. The link between roller j and roller $j+1$ is denoted as link $j+1$.

To locate the contact point, coordinate ξ is defined here along the curve of each tooth of the sprocket as shown in Fig. 1.1. Each point at which two different curves meet is assigned an integer from – 4 to 4 from the left end to the right end of each tooth. The coordinate has a linear scale within each segment. When ξ is used with a subscript, it denotes the ξ coordinate of the corresponding roller.

The typical relationship between ξ_{j+1}, the ξ coordinate of the contact point of roller $j+1$,

and ξ_j, that of roller j, is shown in Fig. 2.2. The graph was obtained for a single pitched roller chain with pitch of 0.5 inch and matching sprockets of 12, 24, and 36 teeth. The graph is symmetric about line $\xi_{j+1} = -\xi_j$. An analytical procedure to compute the location of a roller from that of neighboring roller can be found in Kim [7].

Obviously, the contact points of all the rollers on the sprocket can be located if any one of them is somehow known. Fig. 2.3 illustrates graphically how to determine ξ_2, ξ_3, and so on sequentially from the values of ξ_1 in two different cases. It can be noticed that the distributions of contact points of the two cases shown in Fig. 2.3 are quite different from each other.

In fact, if ξ_R and ξ_L are ξ coordinates of points R and L shown in Fig. 2.3 respectively, the series $\xi_1, \xi_2, ..., \xi_m$ can be classified by the five cases as follow:

Case I If $\xi_1 > \xi_R$, then $\xi_j > \xi_{j-1}$ $(j = 2, 3, ..., m)$

Case II If $\xi_1 = \xi_R$, then $\xi_2 = \xi_3 = ... = \xi_m = \xi_R$

Case III If $\xi_R > \xi_1 > \xi_L$, then $\xi_j < \xi_{j-1}$ $(j = 2, 3, ..., m)$ and converges to ξ_L.

Case IV If $\xi_1 = \xi_L$, then $\xi_2 = \xi_3 = ... = \xi_m = \xi_L$

Case V If $\xi_1 < \xi_L$, then $\xi_j > \xi_{j-1}$ $(j = 2, 3, ..., m)$

It can be observed that the series are characterized by the two specific points marked as R and L in Fig. 2.2 and 2.3. They will be called the "transition points" from here on. The ξ coordinates of the transition points, ξ_R and ξ_L, can be computed analytically. The algorithm to compute the transition point ξ_R is listed in Kim [7]. Note that $\xi_L = -\xi_R$.

For a chain and a sprocket which have exact reference dimensions, the transition points stay in the working curves very close to the border between the seating curve and the working curve ($\xi = 1$ or -1). The locations of the transition points can be affected by the changes in the chain pitch, the sprocket pitch, and the radius of the working curve. Chain pitch, sprocket pitch, and the radius of the working curve of a real sprocket can differ from

the reference values due to manufacturing errors and wear. Chain pitch and the radius of the working curve change in the course of operation due to wear; sprocket pitch is not affected by wear.

The transition points move further toward the inside of the working curves as the chain pitch increases (equivalently, as the sprocket pitch decreases) and as the radius of the working curve increases. Fig. 2.4 shows the location of transition point R of 12-tooth and 24-tooth sprockets for No. 40 and No. 80 chains. The ranges of tolerance on the chain pitch covered in Fig. 2.4 is the same as those allowed by the standard.

Distribution of contact points is not determined solely by the geometrical relationship. It is determined only when the equilibrium equations of the system derived in Section 3 are solved along with the geometrical relationship. Therefore, discussion on the five cases of contact point distribution is continued in Section 4 after the force and moment equilibrium of the system is discussed in Section 3.

3 QUASI-STATIC EQUILIBRIUM OF THE CHAIN AND THE SPROCKET IN CONTACT

In this section, quasi-static force and moment equilibrium of the chain and the sprocket in contact is derived. The friction forces and torques appearing in the equilibrium equations are modeled in accordance with the laws of Coulomb friction.

It is shown that the kinematic variables appearing in the equilibrium equations can be computed if the location of any one of the contact points on the sprocket and the direction of its instantaneous movement are known. It is also shown that the equations can be solved under certain conditions including the case of practical interest where tensions of two chain spans wrapping the sprocket are given. A closed form solution is not available since some of the equations governing the relationship between the kinematic variables are highly non-

linear. The equations can be solved numerically by iteration at any instant or, equivalently, at any sprocket angle. The procedure for the solution is also presented.

3.1 Equilibrium Equations

Equations governing quasi-static equilibrium of each element in Fig. 3.1 are derived. Both scalar variables and vector variables are used to denote forces and torques. Vector quantities will be represented by bold characters and the scalar quantities by plain characters.

Several angles and three sets of unit vectors shown in Fig. 3.2 are used. Definitions of angles are shown in Fig. 3.2. Vectors $\mathbf{x}_j$ and $\mathbf{y}_j$ are unit vectors fixed in tooth j and mutually perpendicular to each other. Vector $\mathbf{y}_j$ is parallel to the axis of symmetry of the tooth. Vector $\mathbf{z}$ is a unit vector equal to $\mathbf{x}_j \times \mathbf{y}_j$. Vector $\boldsymbol{\rho}_j$ is a unit vector normal to the tooth surface directing from outside to inside at the contact point with roller j. Vector $\boldsymbol{\tau}_j$ is perpendicular to normal vector $\boldsymbol{\rho}_j$. Vectors $\boldsymbol{\rho}_j$ and $\boldsymbol{\tau}_j$ are obtained by rotating unit vectors $\mathbf{x}_j$ and $\mathbf{y}_j$ respectively by angle β_j counter-clockwise. Similarly, unit vectors $\mathbf{t}_j$ and $\mathbf{v}_j$ are obtained by rotating unit vectors $\mathbf{x}_j$ and $\mathbf{y}_j$ respectively by angle α_j counter-clockwise. All angles are measured with respect to axis $\mathbf{x}_j$ and defined positive counter-clockwise.

The formulas derived in this section may be sensitive to the orientation. From here on, subscripts i–2, i, i+2, and so on will be used to denote pin links and subscripts i–1, i+1, and so on for roller links. The orientation of elements relevant to any term with a subscript which includes i should be in accordance with Fig. 3.1. If the formula is not sensitive to the orientation subscript j instead of i is used.

Let N_j and F_j be respectively the normal and the tangential components of the contact force on the sprocket by roller j. Rollers i and i+1 are connected to roller link i+1 as shown in Fig. 3.1. Let $\mathbf{Q}_j$ and S_j ($j = i, i+1$) be respectively the resultant force vector passing

through the center of roller j and the accompanying torque in the **z** direction on roller j by roller link i+1. From the free body diagram of roller j in Fig. 3.1 we have

$$\mathbf{Q}_j = N_j \boldsymbol{\rho}_j + F_j \boldsymbol{\tau}_j \quad (j = i, i+1) \tag{3.1}$$

$$S_j = R_R F_j \quad (j = i, i+1) \tag{3.2}$$

where R_R is the radius of the roller.

Let the contact force by link j–1 on link j passing through the center of the joint be $\mathbf{P}_j$ and the magnitude of the accompanying torque in **z** direction be U_j. Equilibrium for pin link i yields

$$\mathbf{P}_{i-1} = \mathbf{P}_i \tag{3.3}$$

$$U_{i-1} - U_i + p_C \mathbf{v}_i \cdot \mathbf{P}_i = 0 \tag{3.4}$$

where p_C is chain pitch. And, for roller link i+1, we have

$$\mathbf{P}_{i+1} + \mathbf{Q}_i + \mathbf{Q}_{i+1} = \mathbf{P}_i \tag{3.5}$$

$$-p_C \mathbf{v}_{i+1} \cdot \mathbf{Q}_i - S_i - U_{i+1} - S_{i+1} = -p_C \mathbf{v}_{i+1} \cdot \mathbf{P}_i - U_i \tag{3.6}$$

Supplementary information on the relationship connecting the tangential forces and the torques to the normal forces is necessary for the equilibrium equations derived above to be solved. This information is supplied from the following friction model.

3.2 Friction Model

Relative motion, or sliding, among the elements of the chain and between the roller and the sprocket is necessary to satisfy the kinematic requirement for the continued motion of the sprocket and the chain. Sliding can occur on the surfaces between the tooth and the roller, between the roller and the bushing, and between the bushing and the pin.

Angle η, the angle between two consecutive chain links, changes as the location of the

contact point changes. The pin should slip against the bushing to accommodate the change in angle η.

Any contact force passing through the contact point can be replaced by the same force whose line of action passes through the pin center and an additional torque. The magnitude of torque U_j can be expressed as

$$U_j = \text{sign}\,(\dot{\eta}_j)\,\frac{\mu_{PB}}{\sqrt{1+\mu_{PB}^2}}\,R_P\left|\mathbf{P}_j\right| \quad (j = i, i+1) \tag{3.7}$$

in which μ_{PB} is the coefficient of kinetic friction between the pin and the bushing and R_P is the radius of the pin, and the operator sign $(\cdot)$ is defined as

$$\text{sign}\,(x) = \begin{cases} 1, \text{ if } x > 0 \\ 0, \text{ if } x = 0 \\ -1, \text{ if } x < 0 \end{cases} \tag{3.8}$$

Note that the friction torque U_j is not determined by Eq. 3.7) when there is no relative motion of the pin against the bushing. Although this may happen in a chain drive operating at extremely slow speeds or exercising intermittent motion, it will not be considered here.

The roller can roll either with slip or without slip on the tooth surface. It is assumed here that the roller slides, if it does, only on either the surface of the sprocket tooth or that of the bushing.

If roller j slips on the tooth surface, the magnitude of the friction force $F_j\boldsymbol{\tau}_j$ on the sprocket by the roller j is equal to $\mu_{RS}\,N_j$ where μ_{RS} is the coefficient of kinetic friction between the roller and the sprocket. The direction of friction force F_j is determined by the direction of the motion of the contact point on the roller relative to the contact point on the sprocket. Let the instantaneous angular velocity of the roller which is assumed to roll without slip be $\dot{\theta}$. Then, the direction of the relative motion of roller j, which this time slides on the sprocket, is determined by sign $(\dot{\alpha}_j - \dot{\theta}_j)$ if link j is a roller link, and by sign $(\dot{\gamma}_j - \dot{\theta}_j)$ if link j is a pin link. And it holds $F_j = F_j^S$ where

$$F_j^S = \begin{cases} \text{sign}\,(\dot{\gamma}_i - \dot{\theta}_i)\,\mu_{RS}\,N_j & \text{for } j = i \\ \text{sign}\,(\dot{\alpha}_{i+1} - \dot{\theta}_{i+1})\,\mu_{RS}\,N_j & \text{for } j = i+1 \end{cases} \tag{3.9}$$

in which μ_{RS} is the coefficient of kinetic friction between the roller and the sprocket. Torque S_j is determined from Eq. (3.2).

If roller j rolls without slip on the tooth surface, sliding occurs between the roller and the respective bushing. In this case, resultant force $\mathbf{Q}_j$ passing through the roller center and the accompanying torque S_j on the roller by the bushing will have a similar relationship to that between force $\mathbf{P}_j$ and torque U_j. That is, it holds $S_j = S_j^B$ where

$$S_j^B = \begin{cases} \text{sign}\,(\dot{\gamma}_i - \dot{\theta}_i)\,\dfrac{\mu_{BR}}{\sqrt{1+\mu_{BR}^2}}\,R_B\,|\mathbf{Q}_i| & \text{for } j = i \\ \text{sign}\,(\dot{\alpha}_{i+1} - \dot{\theta}_{i+1})\,\dfrac{\mu_{BR}}{\sqrt{1+\mu_{BR}^2}}\,R_B\,|\mathbf{Q}_{i+1}| & \text{for } j = i+1 \end{cases} \tag{3.10}$$

where μ_{BR} is the coefficient of kinetic friction between the bushing and the roller and R_B is the outer radius of the bushing. Friction force F_j and torque S_j can be expressed in terms of normal force N_j from the simultaneous solution to $S_j = S_j^B$, Eq. (3.1), (3.2), and (3.10). This leads to $F_j = F_j^B$ where

$$F_j^B = \begin{cases} \text{sign}\,(\dot{\gamma}_i - \dot{\theta}_i)\,\dfrac{R_B\,\mu_{BR}}{\sqrt{R_R^2 + \mu_{BR}^2\left(R_R^2 - R_B^2\right)}}\,N_i & \text{for } j = i \\ \text{sign}\,(\dot{\alpha}_{i+1} - \dot{\theta}_{i+1})\,\dfrac{R_B\,\mu_{BR}}{\sqrt{R_R^2 + \mu_{BR}^2\left(R_R^2 - R_B^2\right)}}\,N_{i+1} & \text{for } j = i+1 \end{cases} \tag{3.11}$$

If the magnitude of friction force F_j^B is less than F_j^S, sliding occurs between the bushing and the roller. Otherwise, sliding occurs between the sprocket tooth and the roller. In other words, friction force F_j is given by

$$F_j = \kappa_j^F N_j, \quad \kappa_j^F = \begin{cases} \dfrac{F_j^B}{N_j}, \text{ if } \mu_{BR} R_B < \mu_{RS} \sqrt{R_R^2 + \mu_{BR}^2 \left(R_R^2 - R_B^2\right)} \\ \dfrac{F_j^S}{N_j}, \text{ otherwise} \end{cases} \qquad (j = i, i+1) \qquad (3.12)$$

And torque S_j becomes

$$S_j = \kappa_j^S N_j, \quad \kappa_j^S = \frac{R_R F_j}{N_j} = R_R \kappa_j^F \quad (j = i, i+1) \qquad (3.13)$$

The directions of the friction forces and the accompanying torques are determined by sign $(\dot{\eta}_j)$, sign $(\dot{\gamma}_i - \dot{\theta}_i)$, and sign $(\dot{\alpha}_{i+1} - \dot{\theta}_{i+1})$ in Eq. (3.7), (3.9), (3.10) and (3.11). Note that angles α_j, β_j, γ_j, η_j, and θ_j $(j = 1, 2, ..., m)$ except α_1 and γ_m are determined from ξ_j's which in turn can be determined if any one of them, for example ξ_1, is known. Angle α_1 and angle γ_m are determined by the angle of the sprocket with respect to the chain spans.

Due to the geometry of standard chains and sprockets it holds without exception that $\dot{\alpha}_j < \dot{\theta}_j$ unless $j = 1$ and that $\dot{\gamma}_j < \dot{\theta}_j$ unless $j = m$. Thus we have

$$\text{sign}\,(\dot{\alpha}_j - \dot{\theta}_j) = \begin{cases} \text{sign}\,(\dot{\alpha}_1 - \dot{\theta}_1), & \text{if } j = 1 \\ -\text{sign}\,(\dot{\theta}_j) = \text{sign}\,(\dot{\xi}_j) = \text{sign}\,(\dot{\xi}_1), & \text{if } j \neq 1 \end{cases} \qquad (3.14)$$

and

$$\text{sign}\,(\dot{\gamma}_j - \dot{\theta}_j) = \begin{cases} \text{sign}\,(\dot{\gamma}_m - \dot{\theta}_m), & \text{if } j = m \\ -\text{sign}\,(\dot{\theta}_j) = \text{sign}\,(\dot{\xi}_j) = \text{sign}\,(\dot{\xi}_1), & \text{if } j \neq m \end{cases} \qquad (3.15)$$

In other words, the friction forces on the sprocket teeth (except teeth 1 and m) have the same direction as the movement of the contact point of roller 1. The directions of the friction forces on teeth 1 and m are not determined solely from geometrical reasoning. They can also be influenced by instantaneous loading conditions. Computation results obtained for a wide range of conditions indicate that it holds that $\dot{\alpha}_1 > \dot{\theta}_1$ and $\dot{\gamma}_m > \dot{\theta}_m$.

However, no presumption about this is necessary to solve the equilibrium equations as will be shown later. Note that sign $(\dot{\alpha}_1)$ = sign $(\dot{\gamma}_m)$ = -1. The friction force on each tooth except tooth 1 and tooth m is toward the direction of decreasing ξ in Case III; it is toward the direction of increasing ξ in Cases I and V.

3.3 Solution Procedure

Let the components of force $\mathbf{P}_j$ parallel to unit vectors $\mathbf{t}_j$ and $\mathbf{v}_j$ be T_j and V_j respectively. That is,

$$\mathbf{P}_j = T_j \mathbf{t}_j + V_j \mathbf{v}_j \quad (j = i, i+1) \tag{3.16}$$

From Eq. (3.4), (3.7), and (3.16) we have

$$p_C V_i = \left\{\text{sign}(\dot{\eta}_i) - \text{sign}(\dot{\eta}_{i-1})\right\} \frac{\mu_{PB} R_P}{\sqrt{1+\mu_{PB}^2}} \sqrt{T_i^2 + V_i^2} \tag{3.17}$$

Solving Eq. (3.17) for V_i gives

$$V_i = \kappa_i^V T_i, \quad \kappa_i^V = \frac{\left\{\text{sign}(\dot{\eta}_i) - \text{sign}(\dot{\eta}_{i-1})\right\} \mu_{PB} R_P / p_C}{\sqrt{1 + \mu_{PB}^2 + \left\{\text{sign}(\dot{\eta}_i) - \text{sign}(\dot{\eta}_{i-1})\right\}^2 (\mu_{PB} R_P / p_C)^2}} \tag{3.18}$$

κ_{i+2}^V (the ratio of V_{i+2} to T_{i+2}) can be obtained by replacing i+2 for i in Eq. (3.18).

Then, by use of Eq. (3.3) and (3.16) the ratio of V_{i+1} to T_{i+1}, κ_{i+1}^V, can be computed.

$$\kappa_{i+1}^V \equiv \frac{V_{i+1}}{T_{i+1}} = \frac{\left(T_{i+2}\,\mathbf{t}_{i+2} + \kappa_{i+2}^V T_{i+2}\,\mathbf{v}_{i+2}\right) \cdot \mathbf{v}_{i+1}}{\left(T_{i+2}\,\mathbf{t}_{i+2} + \kappa_{i+2}^V T_{i+2}\,\mathbf{v}_{i+2}\right) \cdot \mathbf{t}_{i+1}} = \frac{\sin\eta_{i+1} - \kappa_{i+2}^V \cos\eta_{i+1}}{-\cos\eta_{i+1} - \kappa_{i+2}^V \sin\eta_{i+1}} \tag{3.19}$$

And from Eq. (3.7), (3.16) and (3.18) torque U_j can be expressed as

$$U_j = \kappa_j^U T_j, \quad \kappa_j^U = \text{sign}(\dot{\eta}_j) \frac{\mu_{PB} R_P}{\sqrt{1+\mu_{PB}^2}} \sqrt{1 + \left(\kappa_j^V\right)^2} \quad (j = i, i+1) \tag{3.20}$$

Substituting Eq. (3.16) and (3.1) along with Eq. (3.12) and (3.18) into Eq. (3.5) and considering two components parallel to $\mathbf{t}_{i+1}$ and $\mathbf{v}_{i+1}$ respectively give the following two scalar equations.

$$T_{i+1} - N_i\left(\cos \nu_i - \kappa_i^F \sin \nu_i\right) + N_{i+1}\left(\cos \varphi_{i+1} + \kappa_{i+1}^F \sin \varphi_{i+1}\right)$$
$$= -T_i\left(\cos \eta_i - \kappa_i^V \sin \eta_i\right) \tag{3.21}$$

$$\kappa_{i+1}^V T_{i+1} - N_i\left(\sin \nu_i + \kappa_i^F \cos \nu_i\right) - N_{i+1}\left(\sin \varphi_{i+1} - \kappa_{i+1}^F \cos \varphi_{i+1}\right)$$
$$= -T_i\left(\sin \eta_i + \kappa_i^V \cos \eta_i\right) \tag{3.22}$$

Similarly, Eq. (3.6) can be rewritten as

$$-\kappa_{i+1}^U T_{i+1} + \left\{p_C\left(\sin \nu_i + \kappa_i^F \cos \nu_i\right) - \kappa_i^S\right\} N_i - \kappa_{i+1}^S N_{i+1}$$
$$= \left\{p_C\left(\sin \eta_i + \kappa_i^V \cos \eta_i\right) - \kappa_i^U\right\} T_i \tag{3.23}$$

The three scalar equations, Eq. (3.21) to (3.23), can be solved simultaneously for N_i, N_{i+1}, and T_{i+1} if the values of T_i and the kinematic variables are known.

From Eq. (3.3) and (3.16) we have

$$T_{i+1} = \left(T_{i+2} \cdot \mathbf{t}_{i+2} + V_{i+2} \cdot \mathbf{v}_{i+2}\right) \cdot \mathbf{t}_{i+1} = \left(-\cos \eta_{i+1} - \kappa_{i+2}^V \sin \eta_{i+1}\right) T_{i+2} \tag{3.24}$$

Thus we can express T_{i+2} in terms of T_{i+1} and kinematic variables as

$$T_{i+2} = \frac{T_{i+1}}{-\cos \eta_{i+1} - \kappa_{i+2}^V \sin \eta_{i+1}} \tag{3.25}$$

It is sometimes convenient to use the forces at the mid-points of the chain links instead of the forces at the joints, especially when they are compared with experimental data. Let T_j^* be the tension of the link j at its mass center. Then, from Fig. 3.1, we have

$$T_i^* = \mathbf{P}_i \cdot \mathbf{t}_i = T_i \tag{3.26}$$

$$T_{i+1}^* = \left(\mathbf{P}_{i+1} + \mathbf{Q}_{i+1}\right) \cdot \mathbf{t}_{i+1} = T_{i+1} + \left(\cos \varphi_{i+1} + \kappa_{i+1}^F \sin \varphi_{i+1}\right) N_{i+1} \tag{3.27}$$

Eq. (3.21) to (3.26) hold for all values of j except for link 1 and link m+1 if they are roller links. If link 1 is a roller link, $F_0 = N_0 = 0$ and $\eta_0 = 0$. Then, from Eq. (3.26), (3.22), and (3.23) for i+1 = 1, we have, assuming $U_0 = 0$, the following simultaneous equations for T_1 and N_1.

$$\begin{bmatrix} 1 & \cos\varphi_1 + \kappa_1^F \sin\varphi_1 \\ p_C\,\kappa_1^V - \kappa_1^U & p_C\left(-\sin\varphi_1 + \kappa_1^F \cos\varphi_1\right) - \kappa_1^S \end{bmatrix} \begin{Bmatrix} T_1 \\ N_1 \end{Bmatrix} = \begin{Bmatrix} T_1^* \\ 0 \end{Bmatrix} \tag{3.28}$$

T_1 and N_1 can be computed by solving Eq. (3.28).

If the link m+1 is a roller link, setting $i = m$ and noting that $N_{m+1} = 0$ in Eq. (3.21) and (3.23), we have

$$\begin{bmatrix} 1 & -\left(\cos\nu_m - \kappa_m^F \sin\nu_m\right) \\ 0 & p_C\left(\sin\nu_m + \kappa_m^F \cos\nu_m\right) - \kappa_m^S \end{bmatrix} \begin{Bmatrix} T_{m+1} \\ N_m \end{Bmatrix} = \begin{Bmatrix} -\left(\cos\eta_m - \kappa_m^V \sin\eta_m\right) \\ p_C\left(\sin\eta_m + \kappa_m^V \cos\eta_m\right) - \kappa_m^U \end{Bmatrix} T_m \tag{3.29}$$

It has been shown that values of N_i, T_{i+1}^*, N_{i+1}, and T_{i+2}^* can be determined if we know the value of T_i^* and values of the kinematic variable. A typical problem will be one in which T_1^* and T_{m+1}^* are given. In this case, "searching" for the proper value of ξ_1 which yields the given value of T_{m+1}^* is required, since the positions of the contact points of the rollers are not known.

Since the endless roller chain is composed of roller links and pin links alternately assembled, the behavior of the chain drive cycles with a period of two pitch angles. Thus the solution obtained over two pitch angles represents the complete solution. Numerical solutions can be obtained at any finite number of sprocket angles. Assume that the sprocket angle ϕ is defined so that it increases as the sprocket rotates. An algorithm to obtain the solution at any given value of sprocket angle ϕ is as follows:

Step 1 Assume a value of ξ_1.

Step 2 Determine sign $(\dot{\xi}_1)$ by noting that sign $(\dot{\xi}_1) < 0$ if $\xi_1 < \xi_R$ and sign $(\dot{\xi}_1) > 0$ otherwise.

Step 3 Compute all the angles in Fig. 3.2 at ϕ and ξ_1.

Step 4 Compute also those angles at $\phi + \Delta\phi$ and $\xi_1 + \Delta\xi_1$. $\Delta\phi$ is very small and positive; $\Delta\xi_1$ is very small and positive if sign $(\dot{\xi}_1) > 0$ and negative otherwise. Then,

compute sign $(\dot{\eta}_j)$, sign $(\dot{\gamma}_i - \dot{\theta}_i)$, and sign $(\dot{\alpha}_{i+1} - \dot{\theta}_{i+1})$ in Eq. (3.7), (3.9), (3.10) and (3.11) by assuming that

$$\text{sign}\,(\dot{\eta}) = \text{sign}\left\{\eta\left(\xi_1 + \Delta\xi_1, \phi + \Delta\phi\right) - \eta\left(\xi_1, \phi\right)\right\} \tag{3.30}$$

Step 5 Compute all the forces including T^*_{m+1} by use of equations derived in this section.

Step 6 Compare the computed value of T^*_{m+1} and the given value. If the difference is greater than the given allowance, guess a value of ξ_1 again and repeat step 2 to 4. Repeat this until the difference between the computed value of T^*_{m+1} and the given value falls within a given limit.

Step 4 can be skipped if one uses the facts described by Eq. (3.14) and (3.15) and assumptions that sign $(\dot{\alpha}_1 - \dot{\theta}_1)$ = sign $(\dot{\gamma}_m - \dot{\theta}_m) = -1$ and that sign $(\dot{\eta}_j) = 0$. The first assumption is based on the fact the possible variations in α_1 and γ_m are much larger that those in θ_1 and θ_m. However, the first assumption can be checked and corrected, if necessary. On the contrary, the second assumption corresponds to neglecting the friction torque between the pin and the bushing. Although the error introduced by this approximation may not seriously degrade the accuracy of the computation, use of this approximation is basically a matter of user's discretion.

The computed value of T^*_{m+1} monotonically changes as the value of ξ_1 changes. Therefore, any conventional numerical scheme for the solution of nonlinear equations, such as the bisection method or Newton's method [6], can be incorporated into step 5 to find a satisfactory value of T^*_{m+1}.

4 RESULTS

In this section results obtained by the analysis presented in the previous sections are discussed. First, a general discussion of the result is presented. Then, factors affecting the load distribution of the system are discussed. Finally, the chain tension data for the

experimental system studied by Naji and Marshek in [2,3] are compared with the results obtained by this simulation.

4.1 General

If friction is neglected, Eq. (3.21) to (3.27) are reduced to

$$T_{j+1}^{*} = \frac{\sin \varphi_j}{\sin \nu_j} T_j^{*} \tag{4.1}$$

$$N_j = \frac{\sin\left(\nu_j + \varphi_j\right)}{\sin \nu_j} T_j^{*} \tag{4.2}$$

The ratio between tensions of two adjacent links and the ratio between the normal contact force on the sprocket and the link tension are determined basically by the angles φ_j and ν_j (see Fig. 3.2). Friction changes the ratio slightly. Note that angle φ_j is the angle between link j and the normal vector at the contact point and angle ν_j is the angle between link j+1 and the normal vector. The angles of links j and j+1 with respect to tooth j (angle α_j and γ_j in Fig. 3.2 respectively) are little affected by the change in the location of the contact point. Thus, angles ν_j and φ_j are affected primarily by the location of the contact point of roller j. This implies that locating contact points correctly is very important for accurate prediction of link tensions and contact forces.

The ratio between tensions of two chain spans wrapping the sprocket can be expressed, from Eq. (4.1), as

$$\frac{T_{m+1}^{*}}{T_1^{*}} = \frac{\sin \varphi_1}{\sin \nu_1} \frac{\sin \varphi_2}{\sin \nu_2} \cdots \frac{\sin \varphi_m}{\sin \nu_m} \tag{4.3}$$

All the angles except φ_1 and ν_m shown in the right hand side of Eq. (4.3) can be computed from ξ_1. Angles φ_1 and ν_m are determined from the instantaneous angle of the sprocket with respect to the two chain spans. For fixed φ_1 and ν_m, the tension ratio is a monotonic

function of ξ_1.

In Case I, it holds that $0 < \varphi_j \leq \pi - \nu_j < \frac{\pi}{2}$ $(j = 1, 2, ..., m)$. More specifically, it holds that $\sin \varphi_1 \leq \sin \nu_1$, $\sin \varphi_j < \sin \nu_j$ $(j = 2, 3, ..., m-1)$, and $\sin \varphi_m \leq \sin \nu_m$. The equalities in the first and the third equations hold at the instants of engagement and disengagement respectively. This yields, from Eq. (4.3), that $T^*_{m+1} < T^*_1$. Due to the numbering convention for chain links and the direction of rotation of the sprocket we assumed (as shown in Fig. 2.2) it should be satisfied that $T^*_{m+1} > T^*_1$ for the driven sprocket. Therefore, Case I cannot occur in the driven sprocket. Similarly, it holds that $T^*_{m+1} > T^*_1$ in Case V and cannot occur in the drive sprocket. Cases II and IV would occur if the tension ratio T^*_{m+1}/T^*_1 were to fluctuate according to the periodic changes in the angle of the sprocket, or, angles φ_1 and ν_m. This condition is not met by a normal chain drive in motion. Case III can occur for both the drive sprocket and the driven sprocket.

In Case I, the tension ratio T^*_{m+1}/T^*_1 is smaller than in Case III. Case I occurs in the drive sprocket if the slack tension is extremely low relative to the tight tension and/or only a small fraction of the total number of teeth are in contact with the chain. In this case, the roller moves outside the tooth as the sprocket rotates and derailment can possibly occur (see Fig. 2.3). A similar argument can be made for the driven sprocket in Case V. Obviously Cases I and V do not represent desirable operational conditions. It is possible to compute the value of the tension ratio at which the distribution of contact points transitions from Case I or V to Case III. Case III is the most desirable case and it occurs in most chain drives designed in accordance with conventional design practice.

This line of arguments provides the theoretical basis for the conventional practice of selecting relative shaft position. It is said that the most favorable operating conditions are obtained when the drive approximates the horizontal [9]. It is also recommended that the larger sprocket should be placed in the lower position if the drive is not horizontal. When

the slack span is horizontal, the slack tensions of the two sprockets are positive due to gravity. As the inclination angle of the drive increases, the slack tension of the sprocket in the lower position decreases and it becomes more probable that it will exhibit the contact point distribution of Case I (for a drive sprocket) or Case V (for a driven sprocket) rather than Case III. Since the possibility of having a Case III distribution increases as the number of teeth in contact increases, the larger sprocket should be placed in the lower position. If the condition for a Case III distribution is not satisfied, use of a tensioner sprocket should be considered.

Note that a symmetric distribution of the contact points on the drive sprocket in Case I can be found from a distribution of contact points on the driven sprocket in Case V, in which ξ_j of the drive sprocket is replaced by $-\xi_{m-j}$. Similar arguments can be made for distributions of the contact points of both the drive sprocket and the driven sprocket in Case III. Furthermore, the link tensions and the contact forces on the sprocket can be exactly symmetric (or T_j^* of the drive sprocket is equal to T_{m-j+1}^* of the driven sprocket, etc.), if there were no friction. As was discussed in Subsection 3.2, the directions of the friction forces on the sprocket are not affected by whether the sprocket is the drive sprocket or the driven sprocket. They are determined by the direction of the movement of the contact points on the sprocket and the direction of the rotation of the sprocket. It is assumed that the sprocket rotates counter-clockwise. The contact points on the drive sprocket in Case I move in the same direction as those on the driven sprocket in Case V. In Case III, the roller comes in contact with the sprocket at a point very close to transition point R as it engages with the sprocket. Then it moves toward the other transition point L until it disengages from the sprocket. Thus if friction is involved, symmetry between the drive sprocket and the driven sprocket no longer exists.

4.2 Factors Affecting the Load Distribution

There are several factors that can affect the load distribution of the chain and the sprocket. The effects of the tension ratio of the two chain spans, friction, and the dimensional variations in the chain pitch and the sprocket pitch are discussed in this section. The link tension shown in the figures of this section represents the tension which a link experiences from the instant of engagement to that of disengagement as the sprocket rotates. The angle of rotation in the figures of this section is defined such that it is zero when the link of interest engages with the drive sprocket or when the link disengages from the driven sprocket.[3] Since the two chain spans are assumed to be parallel, the angle of rotation is 180 degrees when the link engages with the driven sprocket and disengages from the drive sprocket. Therefore, the angle of rotation changes from zero to 180 degrees for the drive sprocket and from 180 to zero degrees for the driven sprocket.

The ratio of the slack tension to the tight tension has significant effect on the load distribution of the sprocket and the chain. Fig. 4.1 and 4.2 show the tension of a pin link on the drive sprocket and the driven sprocket respectively. They were obtained with No. 2040 standard steel chains and matching 31-tooth steel sprockets under five different ratios of the slack tension to the tight tension. The same drive and the same tension ratios were used in [2 and 3]. The load distributions have almost the same value up to a certain sprocket rotation angle regardless of the tension ratio. This is because of the fact that the contact points of the first several rollers at the side of the tight tension stay very close to the transition points as shown in Fig. 4.3 and 4.4.

Existence of friction between the bushing and the roller and between the roller and the sprocket makes the load distribution of the drive sprocket different from that of the driven

---

[3]The link tension is maximized when the angle of rotation is zero. The definition of the angle of rotation is the same as used by Naji and Marshek [2, 3].

sprocket. Fig. 4.5 shows the tension of a pin link for various values of the coefficient of kinetic friction for the bushing and the roller. The slack tension is equal to the tight tension in Fig. 4.5. If no friction exists, the tension on the drive sprocket is exactly the same as that on the driven sprocket. The tension drops more quickly after the chain link engages with the drive sprocket as the friction coefficient decreases. The friction between the pin and the bushing has little influence on the load distribution.

The dimensional variations in chain pitch and sprocket pitch significantly affect the load distribution. A negative error in the sprocket pitch showed almost the same influence on the load distribution as a positive error of the same magnitude of the chain pitch. The net error in chain pitch used in Fig. 4.6 is defined as the error in the chain pitch minus the error in the sprocket pitch. The effect of the net error in the chain pitch is reduced as the chain elongates as shown in Fig. 4.6.

Fig. 4.7 and 4.8 show simulated tension of a pin link for one of the chain drives measured by Naji and Marshek in [2 and 3]. The net error in the chain pitch used in the simulation is approximately 0.007 inch per pitch (or 0.084 inch per foot). The coefficient of kinetic friction used in the simulation is 0.08 which is within the typical range for lubricated steel surfaces. Estimated link tension shown in Fig. 4.7 and 4.8 shows an excellent agreement with the measurement by Naji and Marshek (as shown in Fig. 4.9 and 4.10)[4] respectively.

Estimated values of the coefficients of the kinetic friction and the net error in the chain pitch are used in the new analysis for a quantitative prediction of the contact phenomenon in roller chain drives. Estimated values of the coefficients of the kinetic friction and a constant value for the pressure angle were used in previous analyses.

---

[4]Fig. 4.9 and 4.10 are listed here with the permission of Dr. M. R. Naji.

The primary argument in favor of the new analysis is that the net error in the chain pitch can be measured or, at least, related to the physical dimensions of the chain and the sprocket. The effect of the dimensional variations in the chain pitch and the sprocket pitch can be fully appreciated by the new analysis.

Finally, a recent experimental investigation [10] found strong spikes in the chain sideplate force as the point where the roller exits the load sprocket and at the point where the roller enters the motor sprocket. Chain speeds were in the moderate to high range in this study, and this suggests that the load distribution problem may be significantly complicated by dynamic factors (impact and inertia) at higher speeds. This is an excellent area for future research.

5 CONCLUSIONS

The contact phenomenon between a roller chain and sprocket was investigated using a system model which includes significant geometrical detail as well as friction effects. The distribution of the contact points on the sprocket is derived from the model (rather than assumed), hence a logical prediction of the contact phenomenon is possible. Comparison of the simulated link tension with existing experimental data [2, 3] showed an excellent agreement.

It was observed that the distribution of contact points on the sprocket is affected by the external loading condition, and this relationship was determined. The distribution of the contact points can be classified practically into two different cases. In the first case the contact between the chain and the sprocket occurs outside the two points identified as transition points (symmetrically positioned on each tooth). This tends to happen if the ratio of the slack tension to tight tension is extremely low and/or if the number of teeth in contact is small. The load on the sprocket is more concentrated on the first several teeth at the side of the tight span in this case than otherwise. Moreover, the rollers in contact with the

sprocket can be easily stripped out from the sprocket, and the motion of the chain drive can become jerky. This can be avoided by use of an idler sprocket. In the second case, the contact between the chain and the sprocket occurs between the transition points and reliable power transmission is achieved. This condition is satisfied by most chain drives designed in accordance with conventional guidelines on the selection of relative shaft position.

The locations of the transition points vary depending on the dimensional variations in the chain pitch, the sprocket pitch, and the radius of the working curve. Those variations are caused by manufacturing tolerance and wear. The transition points of a roller chain drive with dimensions that correspond to the nominal values given in the ANSI standard [5] reside close to the border with the seating curve. As the chain elongates the transition points move toward the inside of the working curves. But, the transition points of any chain in workable condition will stay within a small portion of the working curve next to the seating curve. The contact points of the first several rollers from the end of the tight span remain very close to the transition point at the side of tight span.

Suggestions for correct interpretation of some terminologies used in the relevant ANSI standard [5] can be made. In the standard the pressure angle[5] is given for different cases. The "pressure angle for a new chain" is denoted as the pressure angle of the inner end point of the working curve (the border point between the working curve and the seating curve). This seems to be a good approximation for the first several rollers from the tight span, since they remain very close to the transition point and the transition point for a new chain resides very close to the inner end point of the working curve. But, it should be also noticed that some of the rollers may contact the seating curve. The "minimum pressure angle" is denoted in the standard as the pressure angle of the outer end point of the working curve. This should not be interpreted as an implication that a fully elongated, but

[5]In fact, the definition of the pressure angle cannot be found from the standard. It is defined in Ref. 1 as the angle φ in Fig. 1.1.

workable, chain may have this small value of the pressure angle.

REFERENCES

1. Binder, R. C., 1956, *Mechanics of the Roller Chain Drive*, Prentice-Hall, Englewood Cliffs, New Jersey.

2. Naji, M. R., 1981, *On Timing Belt and Roller Chain Load Distribution*, Ph. D. Dissertation, University of Houston, Houston, Texas.

3. Naji, M. R. and Marshek, K. M., 1983, "Experimental Determination of the Roller Chain Load Distribution," ASME *Journal of Mechanisms, Transmission, and Automation in Design*, Vol. 105, pp. 331 - 338.

4. Naji, M. R. and Marshek, K. M., 1984, "Analysis of Roller Chain Sprocket Pressure Angles," *Mechanism and Machine Theory*, Vol. 19, No. 2, pp. 197 - 203.

5. American National Standards Institute, 1975, "Precision Power Transmission Roller Chains, Attachments, and Sprockets," ANSI *Standard B29.1 - 1975*, New York.

6. Conte, S. D. and de Boor, Carl, 1972, *Elementary Numerical Analysis*, McGraw-Hill.

7. Kim, M. S., 1990, *Dynamic Behavior of Roller Chain Drives at Moderate and High Speeds*, Ph. D. dissertation, University of Michigan.

8. Gerbert, G., 1989, "Tooth Action in Chain and Timing Belts," *International Power Transmission and Gearing Conference - Vol. 1, Book No. 10288A - 1989*, ASME, NY, pp 81 - 89.

9. Bouillon, G. and Tordion,G. V., 1965, "On Polygonal Action in Roller Chain Drives", *ASME J. Engineering for Industry*, Vol. 87B, pp 243 - 250.

10. Conwell, J. C., 1989, *An Examination of Transient Forces in Roller Chain Drives*, Ph.D. dissertation, Vanderbilt University.

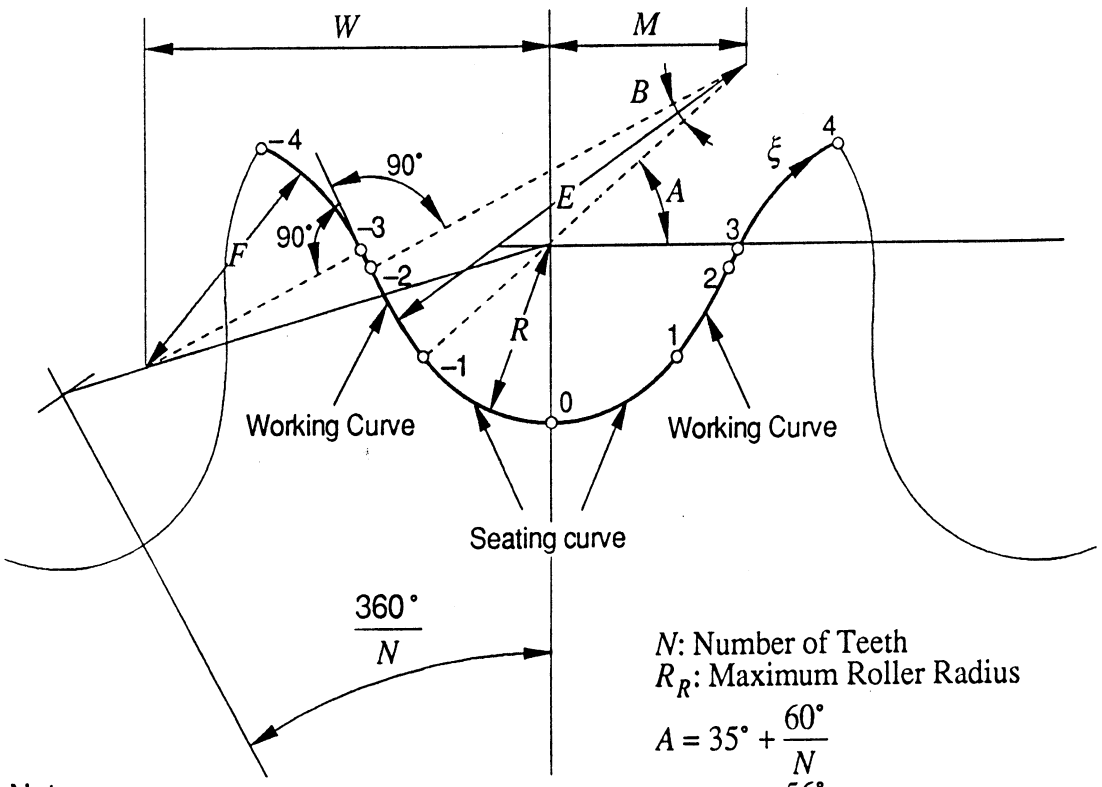

Notes:
1. Coordinate ξ and the integers on the tooth surface are not parts of the standard.
2. E and F can be computed from other constants shown in the right or found from the standard.

N: Number of Teeth
R_R: Maximum Roller Radius

$$A = 35° + \frac{60°}{N}$$

$$B = 18° - \frac{56°}{N}$$

$$R = 1.005\,R_R + 0.0015 \text{ (in inches)}$$

$$M = 1.6\,R\cos A$$

$$W = 2.8\,R\cos\frac{180°}{N}$$

Fig. 1.1 Standard Sprocket Tooth Form for Roller Chains

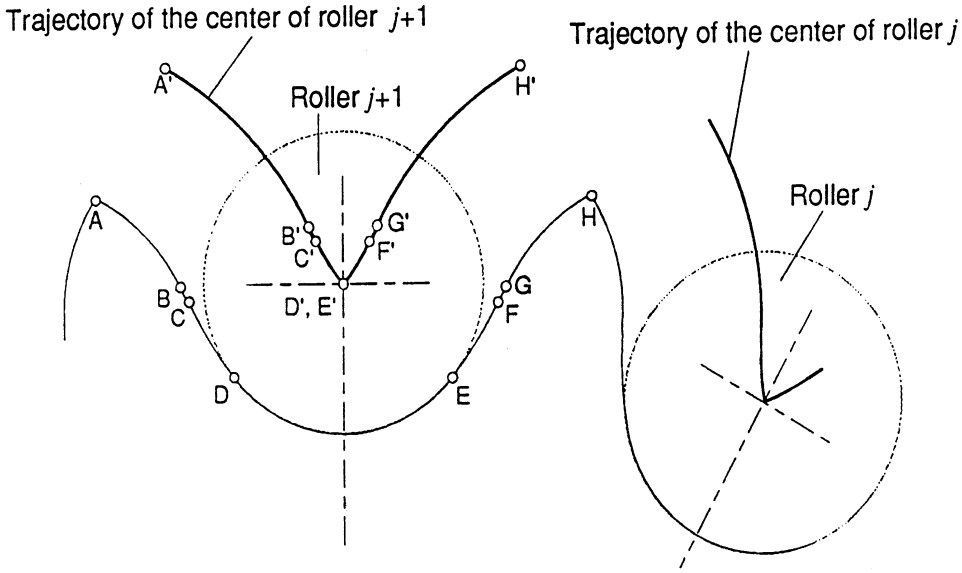

- Radii difference between the roller and the seating curve (curve DE) neglected
- The contact point on the seating curve cannot be determined from physics

(a) Previous Models

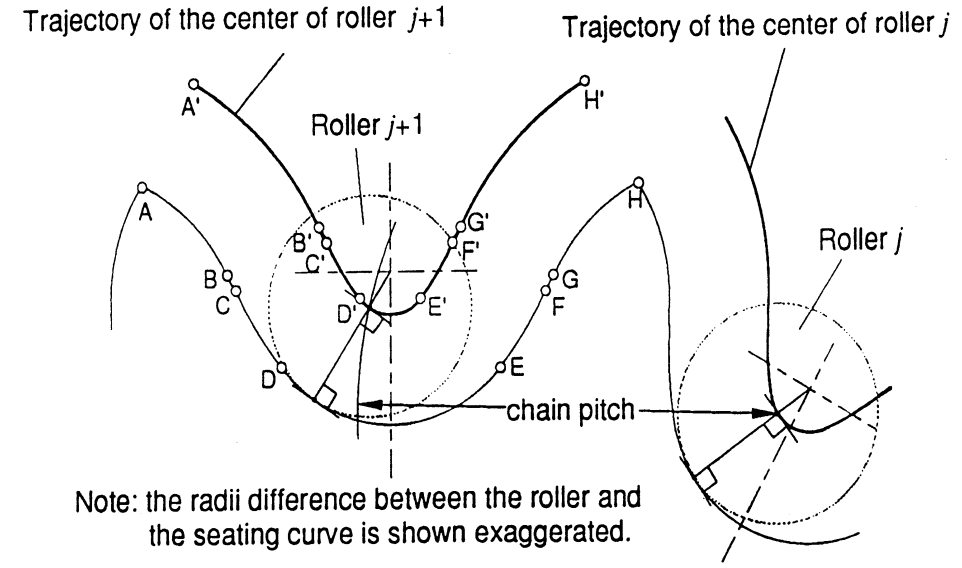

- Radii difference between the roller and the seating curve (curve DE) considered
- Contact point on the seating curve can be located

(b) New Model

Fig. 1.2 Differences in Modeling of the Contact Point on the Seating Curve

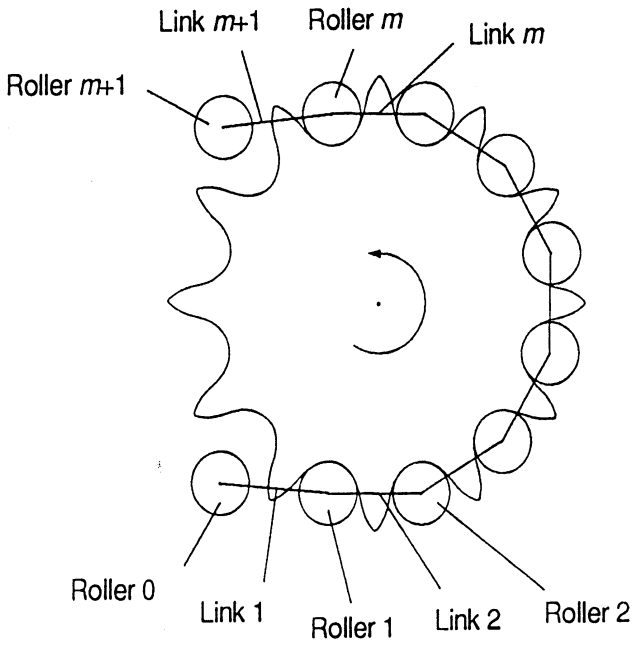

Fig. 2.1 Roller Chain Drive

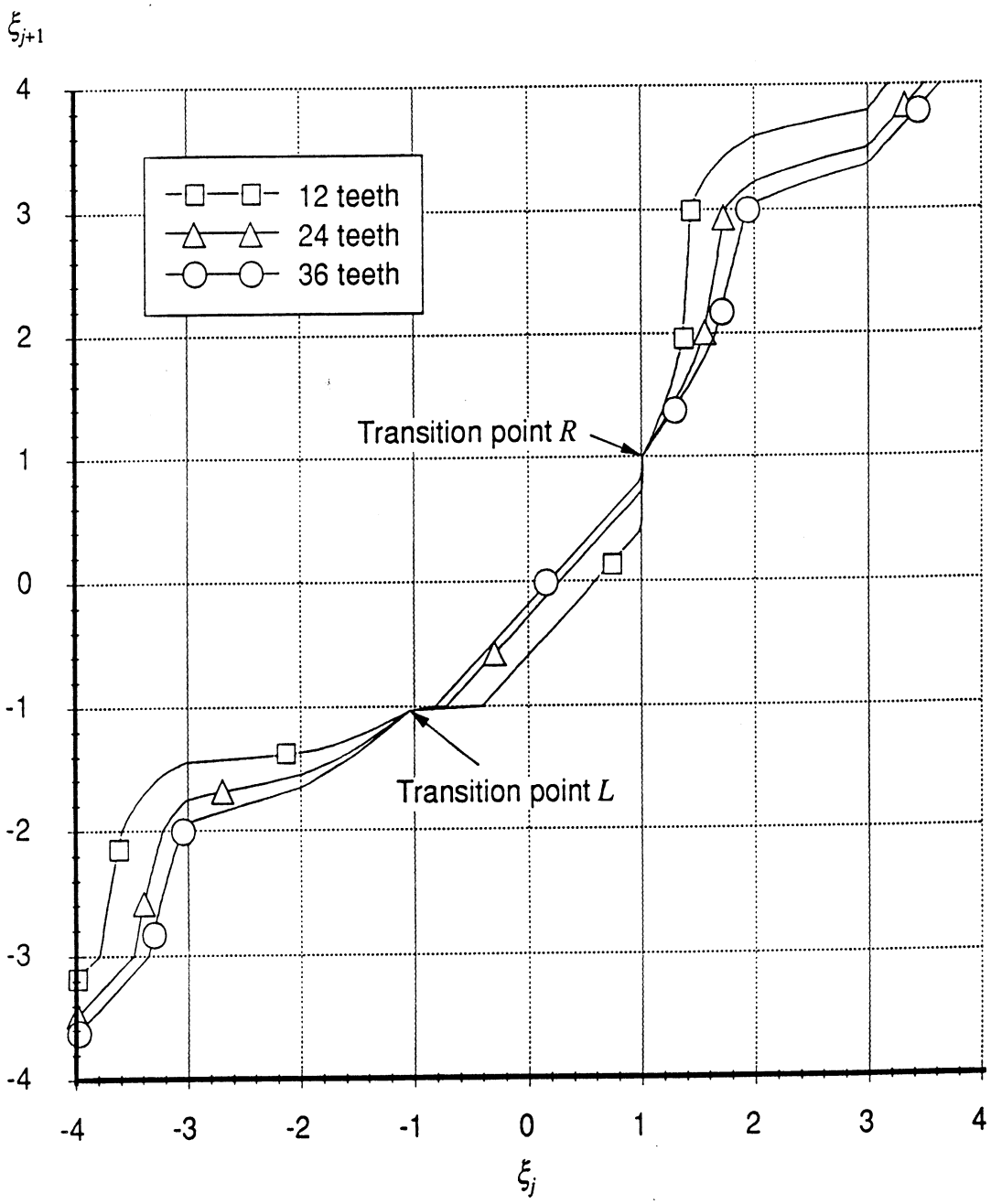

Fig. 2.2 Relationship between the Locations of the Contact Points of Two Adjacent Rollers

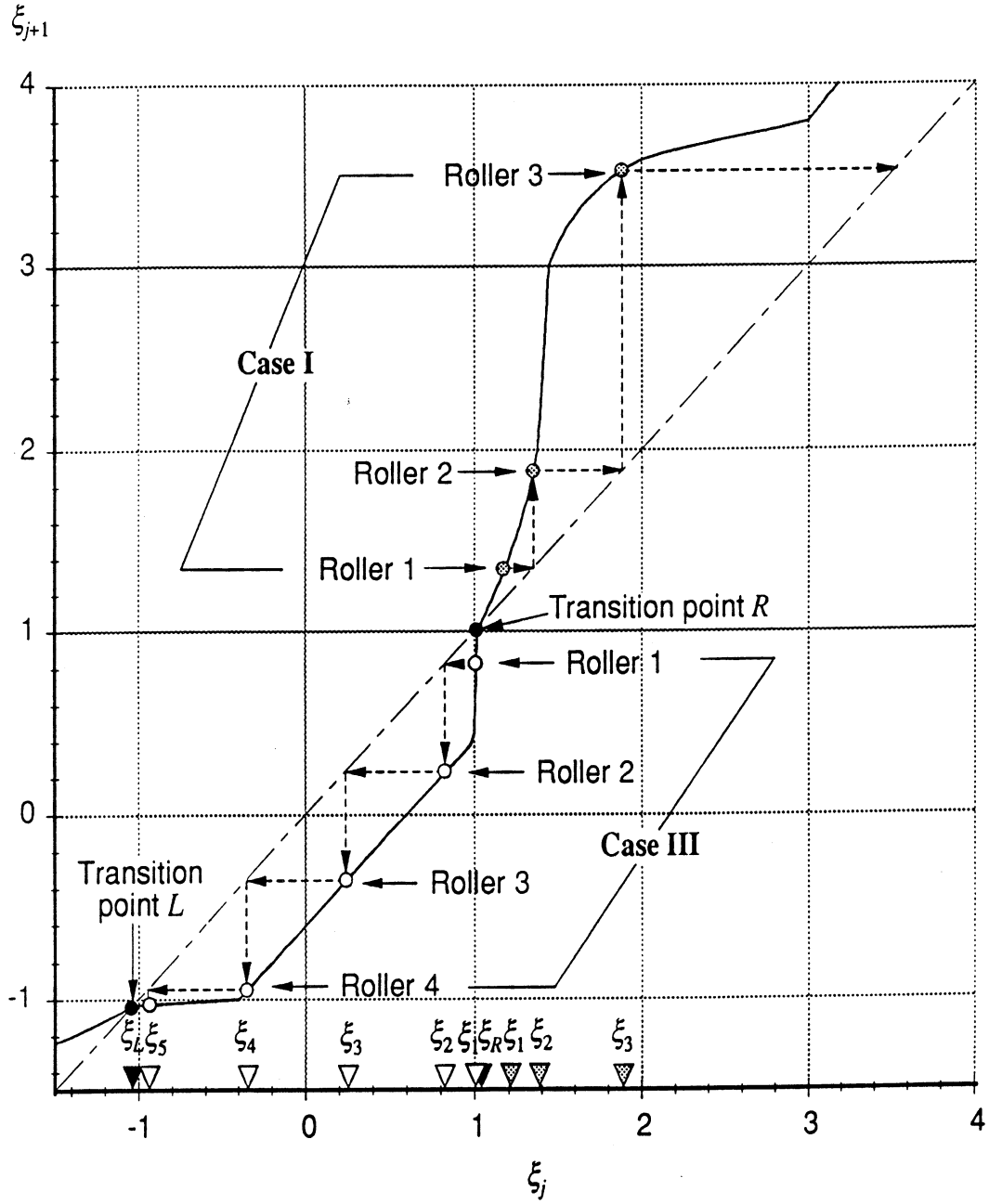

Fig. 2.3 Distribution of Contact Points in Two Typical Cases

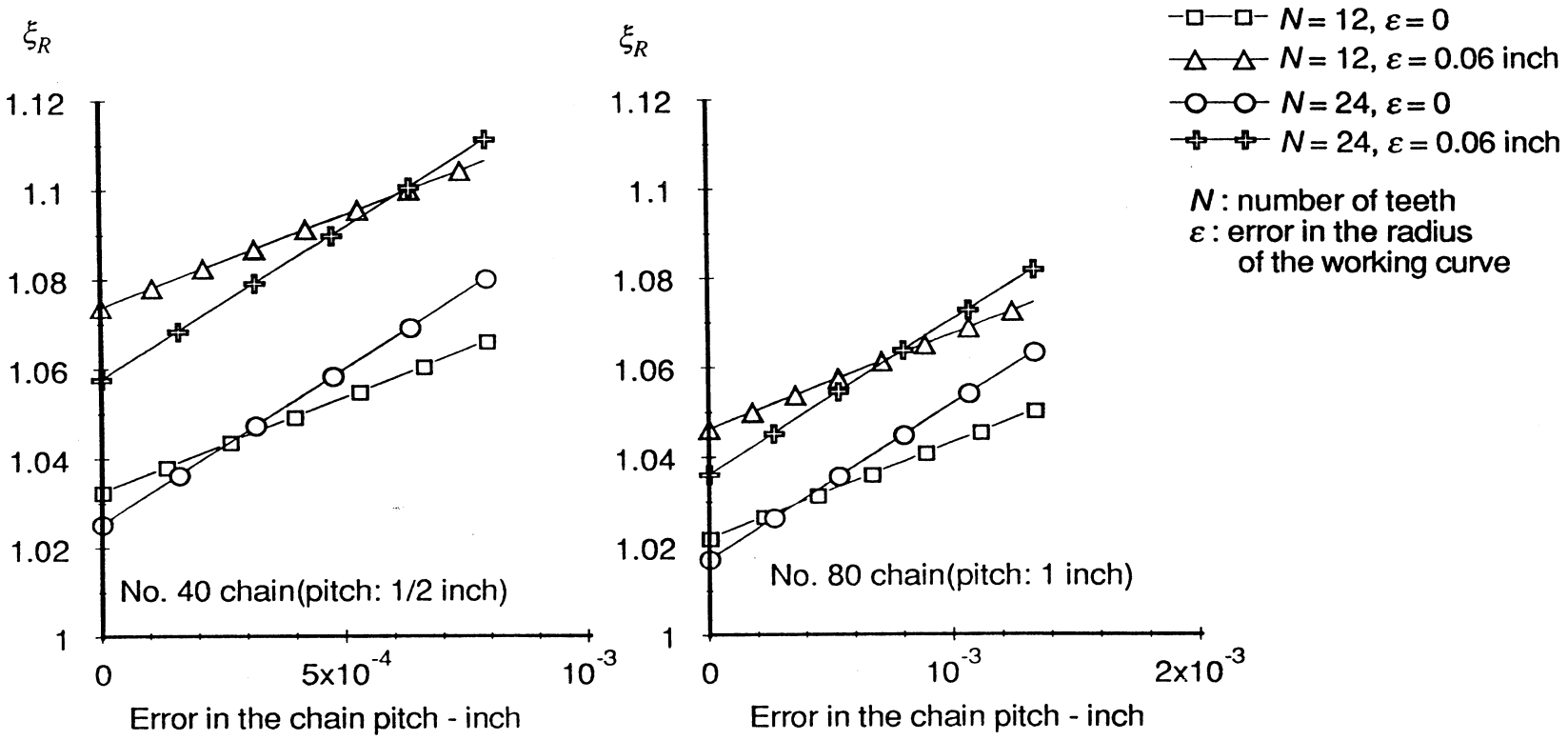

Fig. 2.4 Variations in ξ Coordinate of Transition Point R

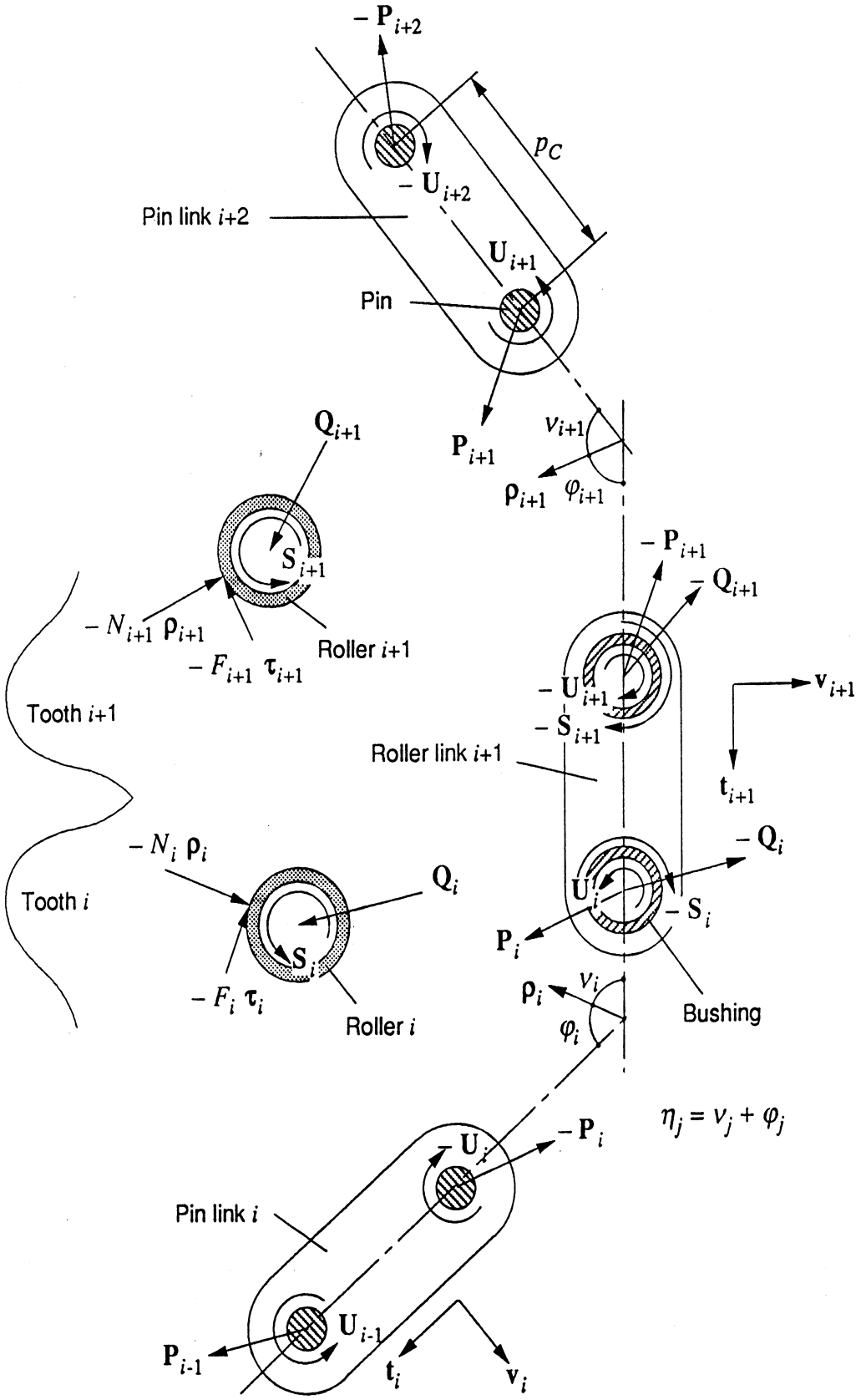

Fig. 3.1 Free Body Diagram of Elements of Roller Chain

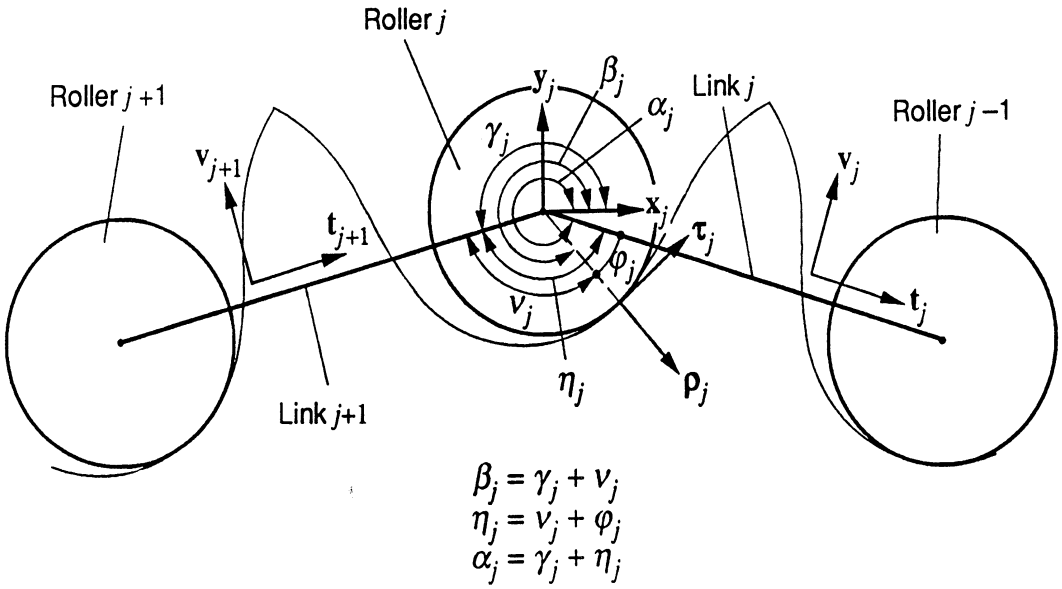

Fig. 3.2 Definition of Angles Related to Roller *j*

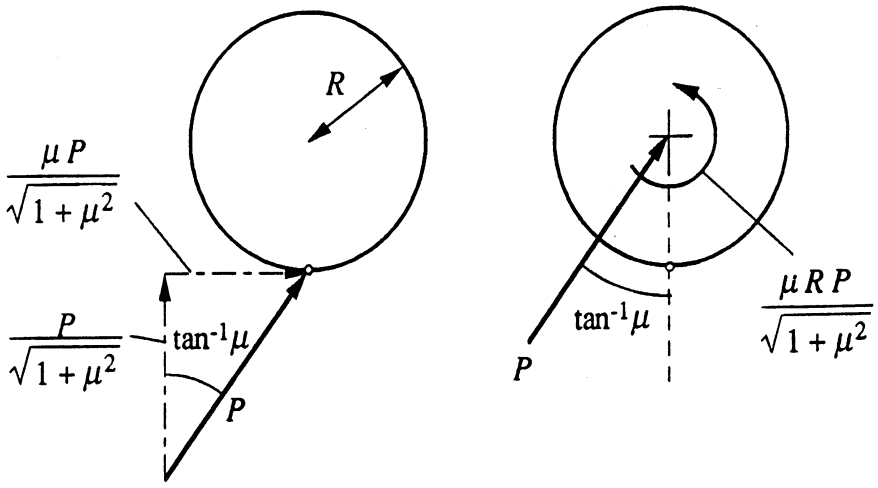

Fig. 3.3 Two Equivalent Contact Loadings on a Cylinder

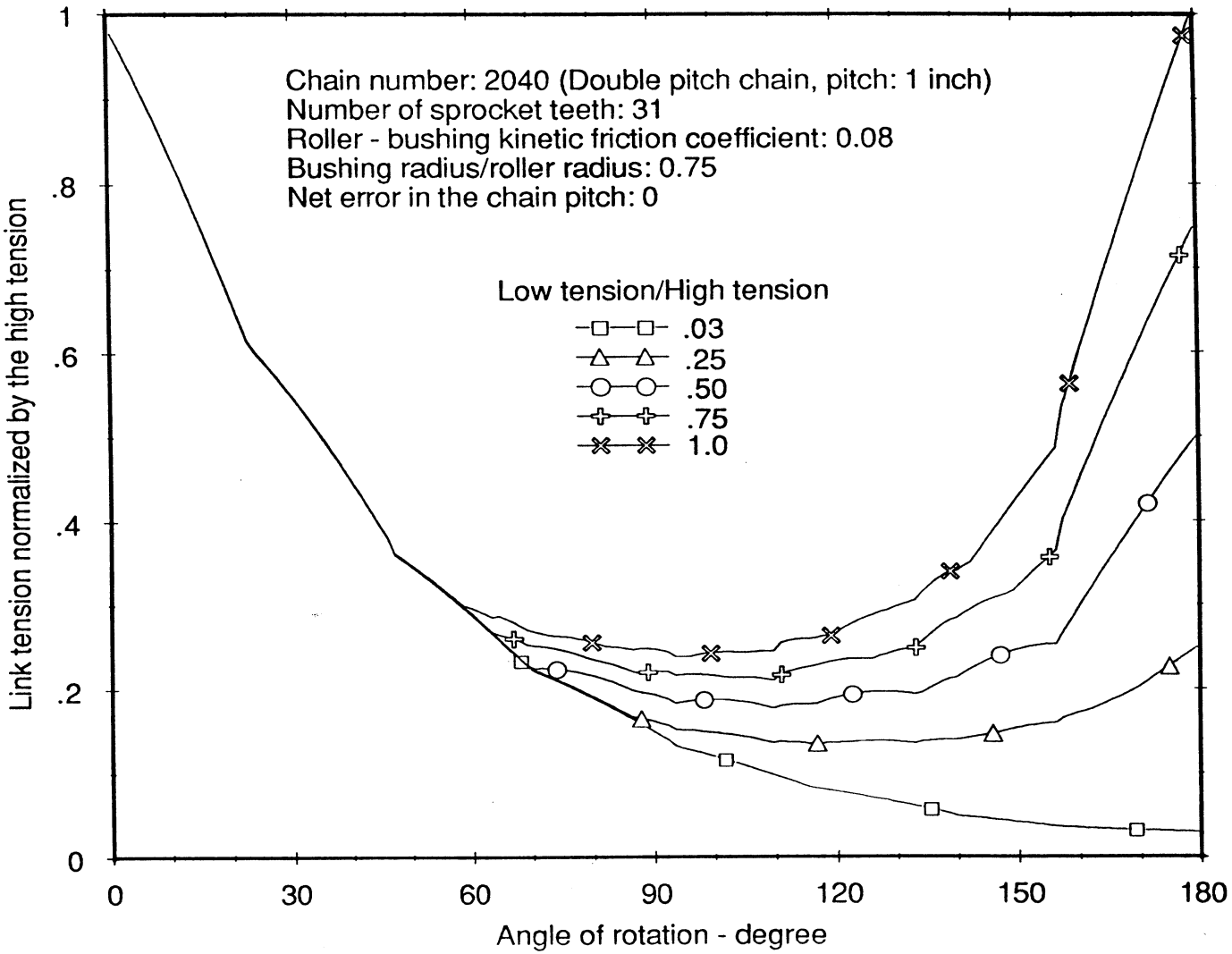

Fig. 4.1 Pin Link Tension on the Drive Sprocket

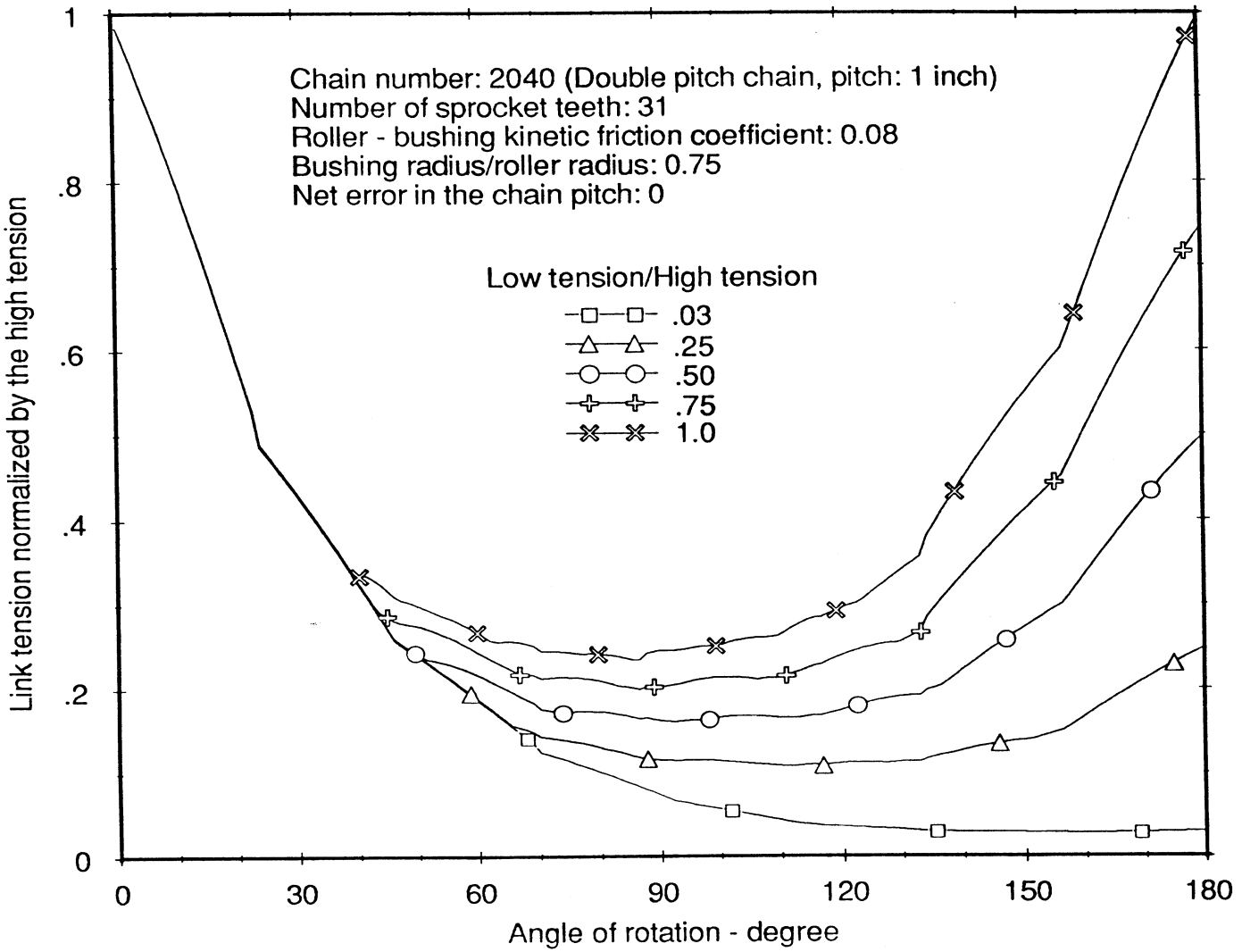

Fig. 4.2 Pin Link Tension on the Driven Sprocket

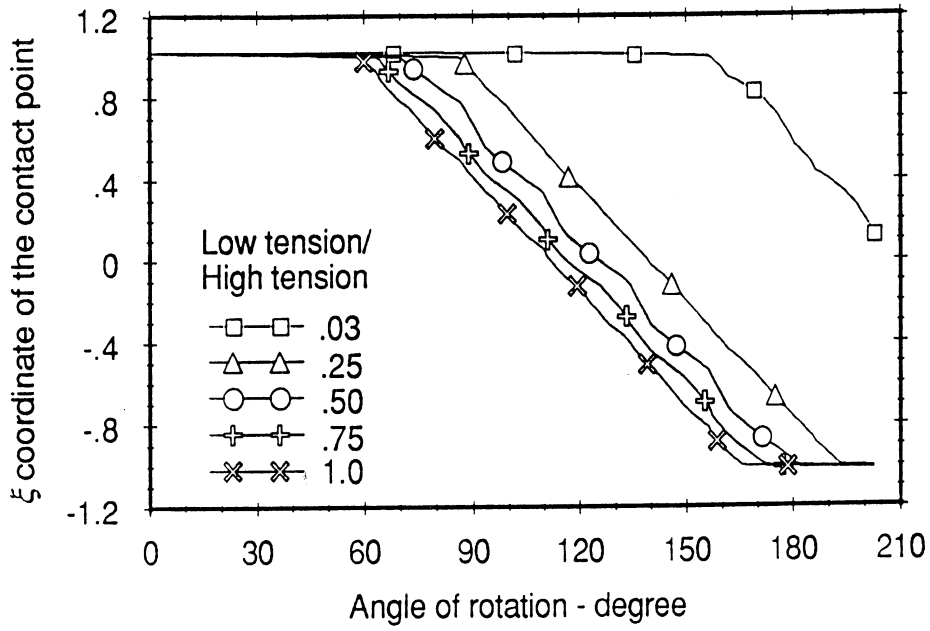

Fig. 4.3 Locations of Contact Points for the System in Fig. 4.1

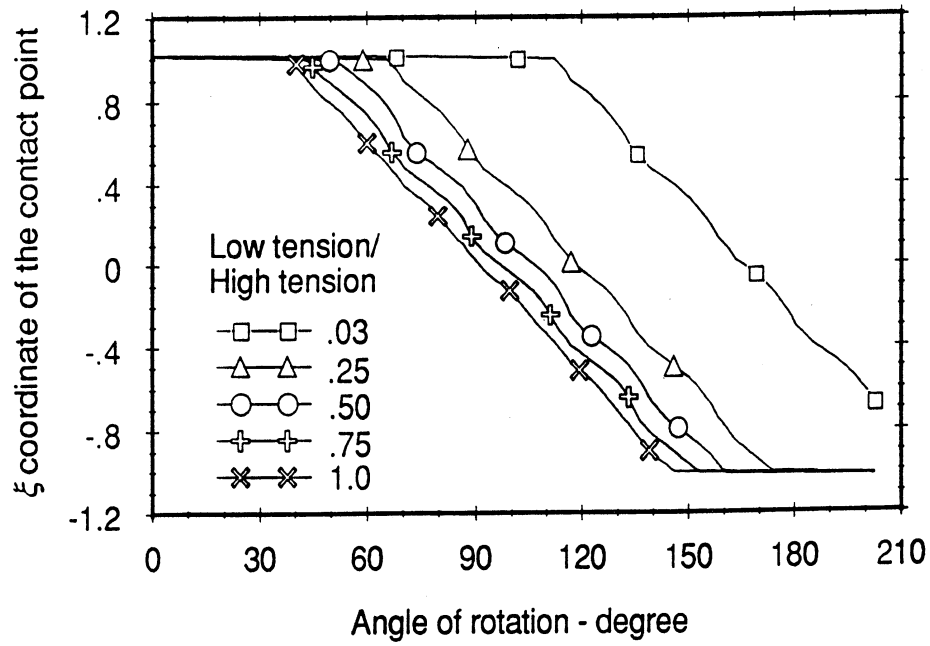

Fig. 4.4 Locations of Contact Points for the System in Fig. 4.2

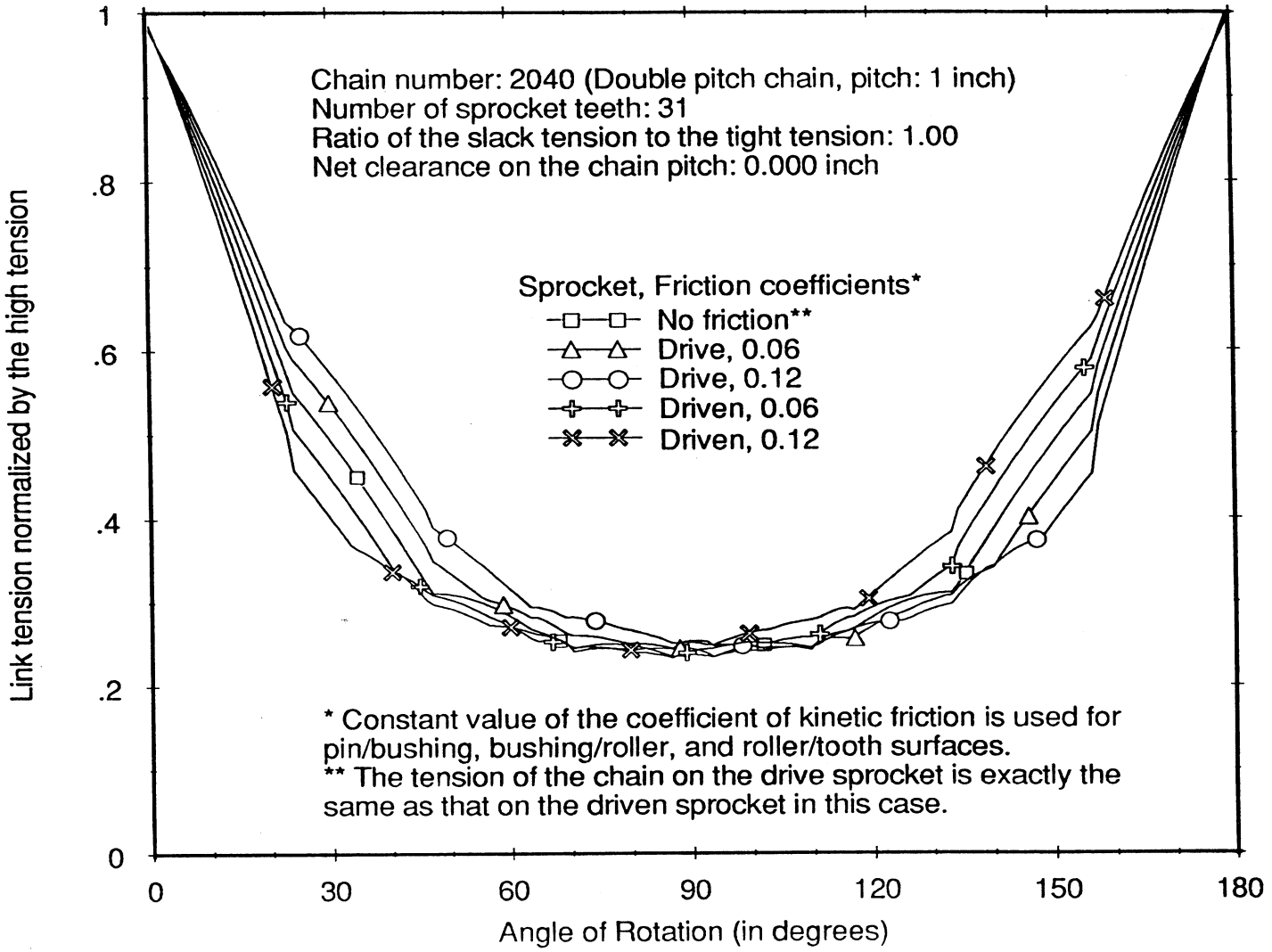

Fig. 4.5 Effects of Friction on Pin Link Tension

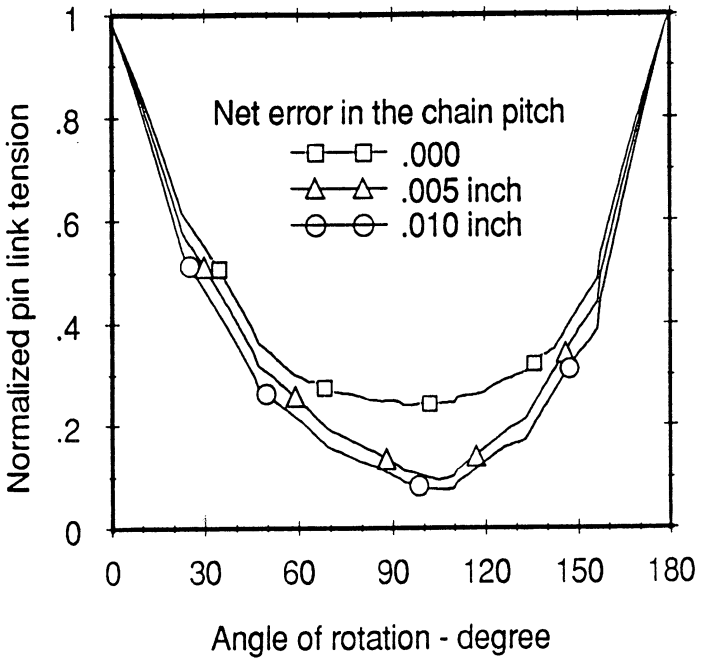

(a) Pin Link Tension on the Drive Sprocket

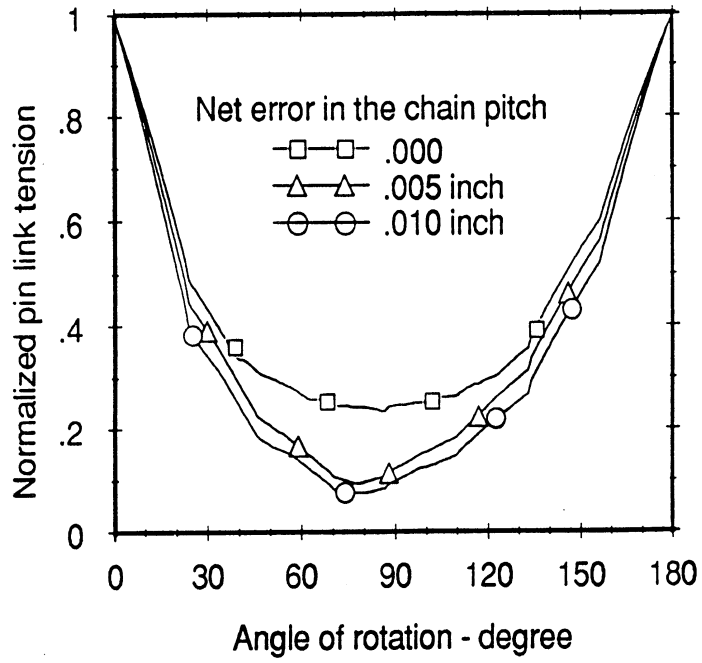

(b) Pin Link Tension on the Driven Sprocket

Fig. 4.6 Effects of the Net Error in the Chain Pitch on Link Tension

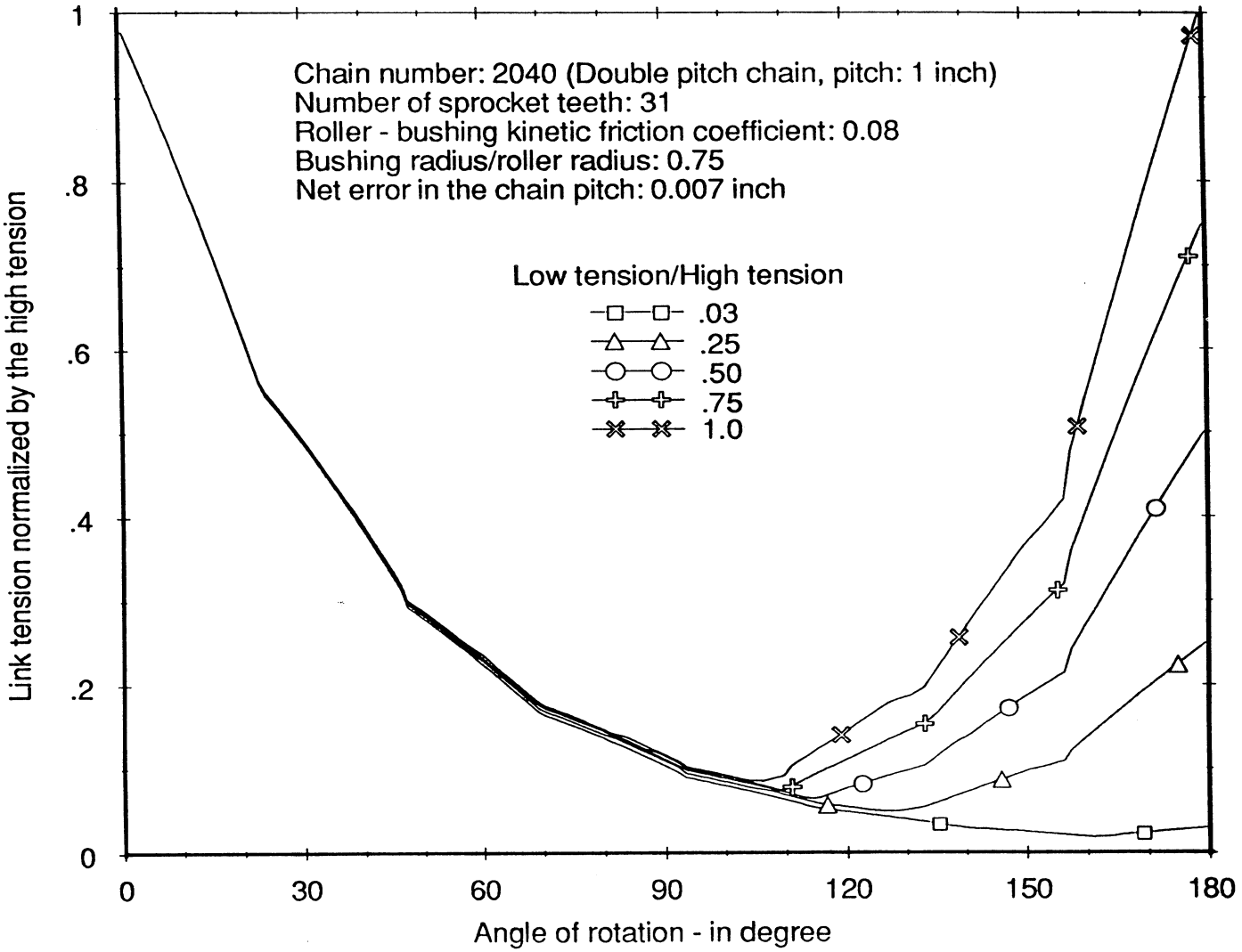

Fig. 4.7 Simulated Pin Link Tension on the Drive Sprocket

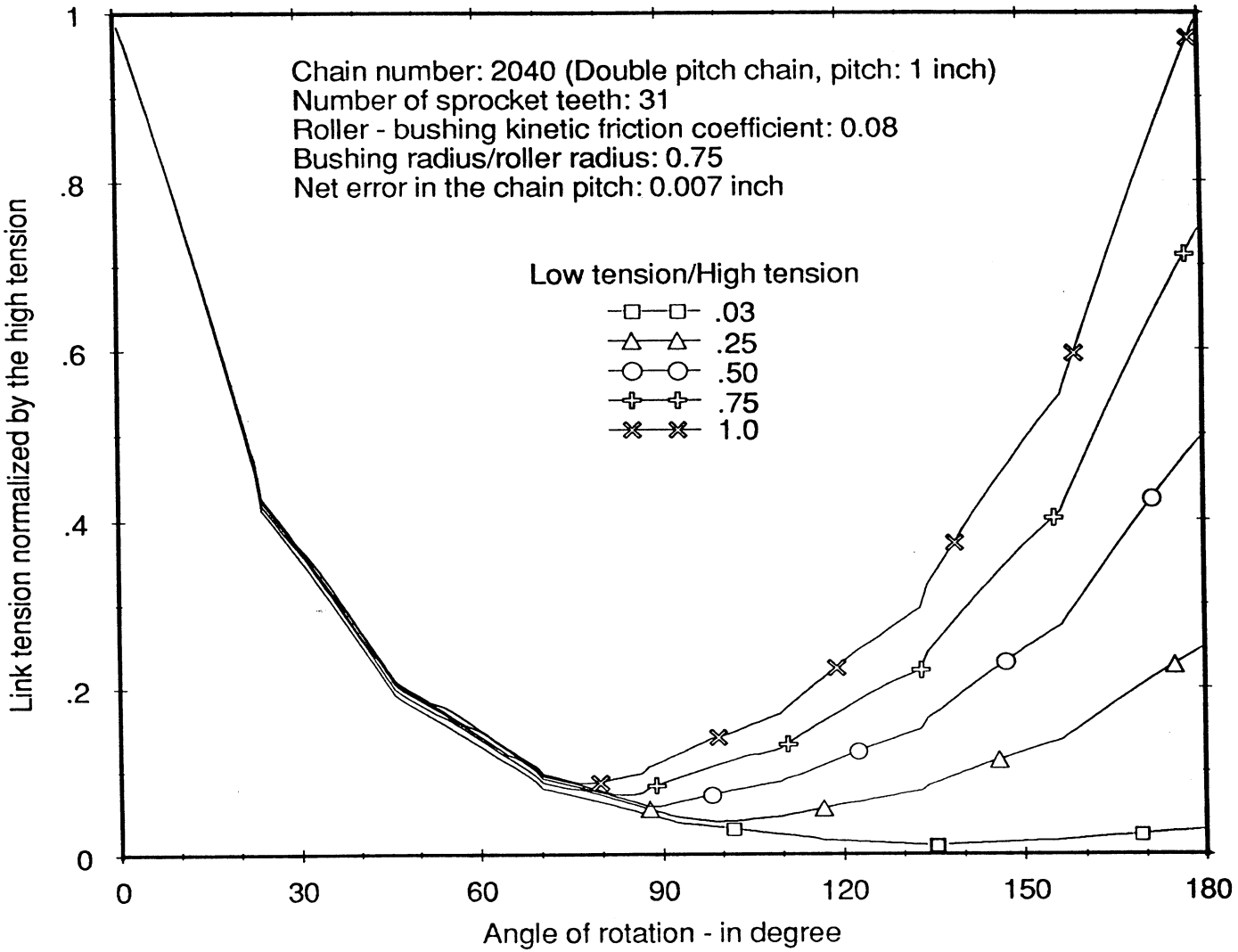

Fig. 4.8 Simulated Pin Link Tension on the Driven Sprocket

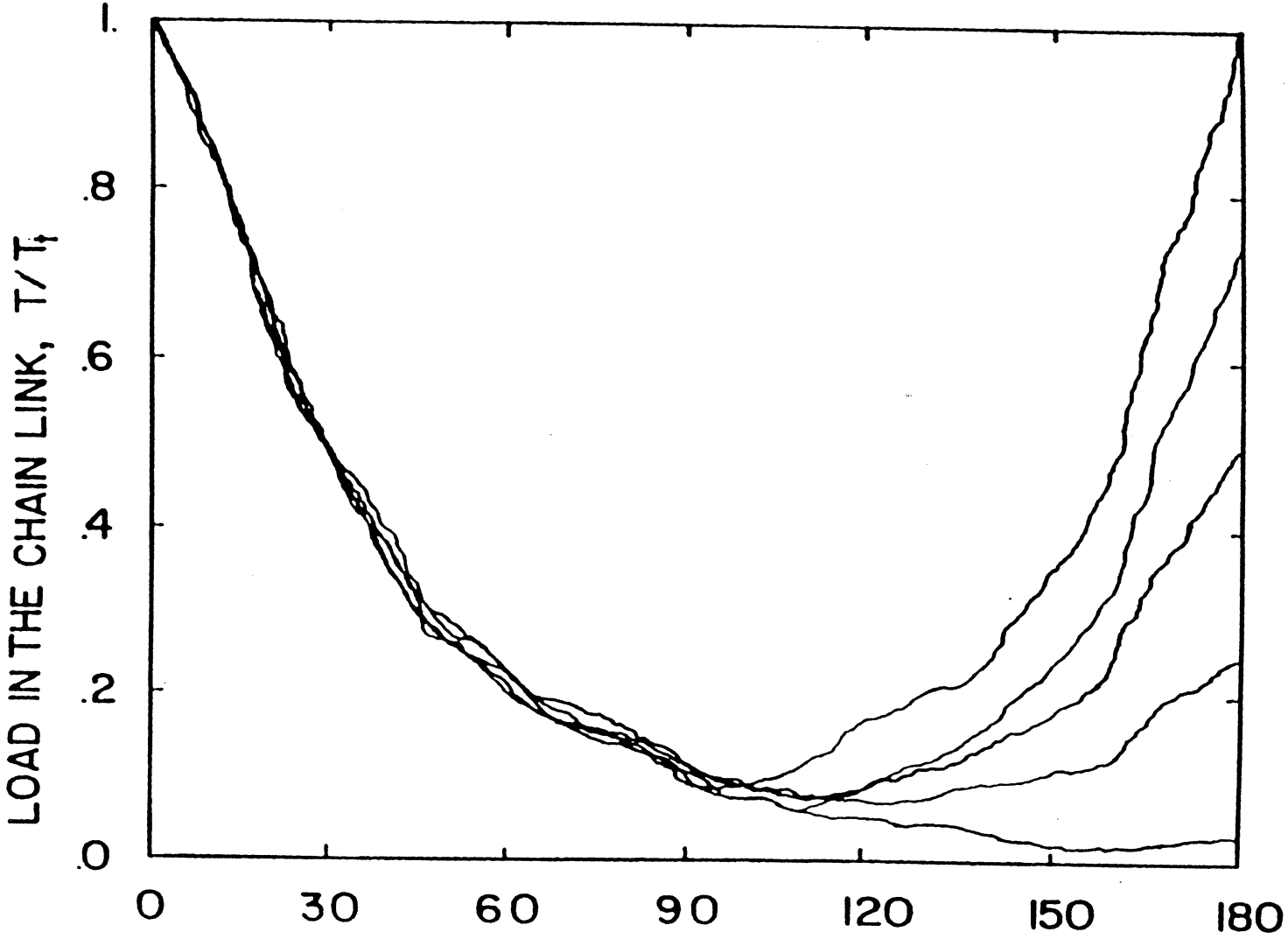

Fig. 4.9 Measured Pin Link Tension on the Drive Sprocket (from Ref. 2)

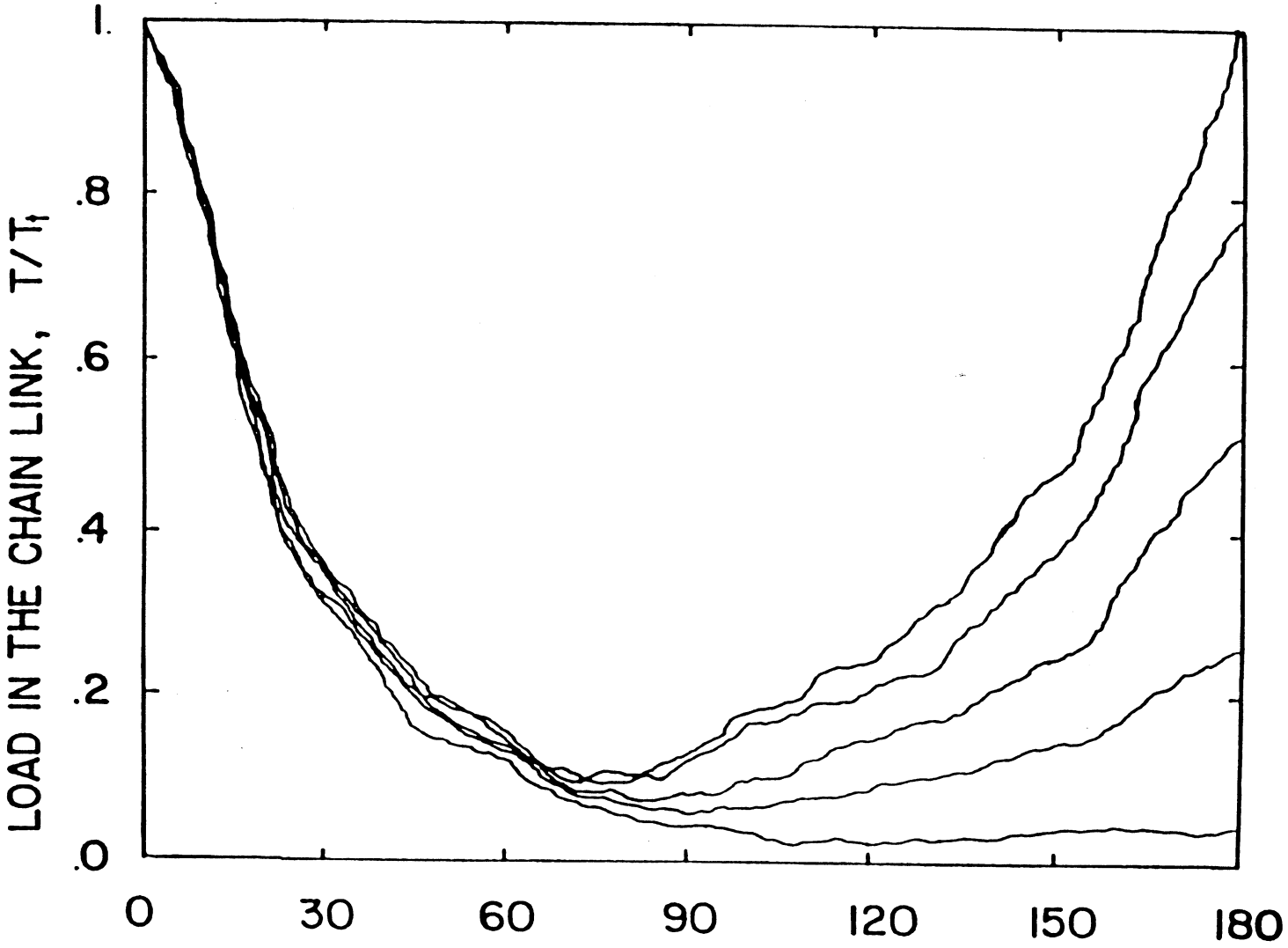

Fig. 4.10 Measured Pin Link Tension on the Driven Sprocket (from Ref. 2)

THE UNIVERSITY OF MICHIGAN

DATE DUE

10-3 17:55	